Chemical Science

ROYAL SOCIETY OF CHEMISTRY

EDGE ARTICLE

Check for updates

All publication charges for this article have been paid for by the Royal Society of Chemistry

Crafting 1,4-diaryl spirobifluorene hosts in OLEDs *via* interannular C−H arylation: synergistic effects of molecular linearity and orthogonality†

Qian Li, Zhiqian Yu, Qianhui Liu, Yusong Guo, Zhangyi Fu, Yudong Yang, [ID] Zhengyang Bin, [ID] Di Wu [ID] * and Jingbo Lan [ID] *

In this work, we present a design concept of introducing linear structures into the orthogonal configuration of 9,9′-spirobifluorene (SBF), aiming to enhance carrier mobilities while maintaining high triplet energies (E_T), which are two critical parameters for optimizing host materials in organic light-emitting diodes (OLEDs). To validate our proposed design, four pivotal model molecules of 1,4-diaryl SBFs were synthesized *via* interannular C−H arylation of bi(hetero)aryl-2-formaldehydes, a task challenging to accomplish using previous synthetic methodologies. The orthogonal configuration and the steric hindrance of SBF lead to high E_T through the conjugation breaking at C1 and C4 positions, rendering 1,4-diaryl SBFs suitable as universal pure hydrocarbon (PHC) hosts for red, green, and blue (RGB) phosphorescent OLEDs (PhOLEDs). Meanwhile, the linearity and relatively good planarity of the *para*-quaterphenyl structure promote high carrier mobilities through orderly intermolecular packing. The synergistic effects of linearity and orthogonality in 1-(*para*-biphenyl)-4-phenyl-SBF result in exceptional device performance with external quantum efficiencies (EQEs) of 26.0%, 26.1%, and 22.5% for RGB PhOLEDs, respectively. Notably, the green PhOLED exhibits minimal efficiency roll-off, positioning its device performances among the state-of-the-art in PHC hosts.

Introduction

9,9′-Spirobifluorene (SBF) comprises two fluorene units connected by a shared spiro carbon atom, and the orthogonal configuration between two fluorenyl planes endows SBF derivatives with good solubilities and thermal stabilities.[1] Of particular interest are multi-aryl SBFs, especially in applications involving electroluminescent devices such as organic light-emitting diodes (OLEDs) and solid-state lasers.[2–5] Multi-aryl SBFs with more modifiable sites provide possibilities for the structural diversity of organic luminescent materials, therefore attracting much attention in recent years.[4,5] The synthesis of multi-aryl SBFs typically involves the electrophilic bromination of fluorene, fluorenone and SBF, followed by Suzuki coupling with arylboronic acid.[1,2] Notably, the C2 position exhibits the highest electrophilic reactivity.[1,2] As a result, there has been a considerable body of research dedicated to exploring SBFs with C2-aryl substitution.[1–5] In contrast, multi-aryl SBFs lacking C2-aryl group have received less attention, primarily due to synthetic challenges, limiting the

exploration of new materials based on SBFs.[2] Typically, the synthesis of unsymmetrical multi-aryl SBFs poses additional complexities, necessitating the introduction of multiple halogen atoms with different reactivities on aromatic rings to accomplish sequential Suzuki coupling.

Multi-aryl SBFs are also an important kind of pure hydrocarbon (PHC) hosts for phosphorescent OLEDs (PhOLEDs).[6,7] Recent studies have shown that incorporating various aryl substituents at specific positions of SBFs enables precise tuning of triplet energies (E_T), concurrently enhancing carrier mobility of target molecules, which are two crucial factors in optimizing universal host materials for red, green, and blue (RGB) PhO-LEDs.[8,9] The incorporation of C2-aryl substituent has been noted to significantly reduce the E_T of SBFs due to electronic coupling (Scheme 1a, **2-Ph-SBF** and **1-pbp-7-p-SBF**). The introduction of an aryl substituent at C1 position exerts a minimal impact on E_T because the large dihedral angle between the fluorene plane and C1-aromatic ring disrupts the π-conjugation (Scheme 1a, **1-mtp-SBF**).[6,10–12] Additionally, the presence of a C4-aryl substituent has a slight effect on E_T, attributed to the steric hindrance-induced partial disruption of conjugation at the C4 position (Scheme 1a, **4-Ph-SBF**).[13–15] Research reported by Jiang, Liao, and Poriel suggests that incorporating *meta*-biphenyl (mbp), and *meta*-terphenyl (mtp) at the C1 position substantially enhances carrier mobility without causing significant alteration to the E_T of host materials.[12] Our recent investigation also demonstrates that the introduction of *para*-biphenyl (pbp)

Key Laboratory of Green Chemistry and Technology of Ministry of Education, College of Chemistry, Sichuan University, 29 Wangjiang Road, Chengdu 610064, People's Republic of China. E-mail: wood@scu.edu.cn; jingbolan@scu.edu.cn

at the C1 position contributes significantly to the carrier mobility.[6] Based on these findings, we envision the simultaneous introduction of aryl substituents at both C1 and C4 positions of SBFs would result in a linear *para*-terphenyl or *para*-quaterphenyl structure, and a good linear structure might hold the potential to facilitate organized packing between molecules, thereby promoting high carrier mobilities while keeping high E_T. Density functional theory (DFT) calculations indicate that the highest occupied molecular orbitals (HOMO) of 1,4-diaryl SBFs are distributed over the whole spirobifluorene skeleton. Meanwhile, their lowest unoccupied molecular orbitals (LUMOs) are mainly localized on the substituted fluorene with slight delocalization to the C4-aryl substituent. This result suggests a partial planarization between the fluorene and the C4-aromatic ring in excited states (Scheme 1b). Calculations demonstrate that these 1,4-diaryl SBFs exhibit high E_T exceeding 2.90 eV, providing potential for their application as universal hosts in RGB PhOLEDs (Scheme 1b).[16,17] In this study, we present a palladium-catalyzed interannular selective *ortho*-C–H arylation of bi(hetero)aryl-2-formaldehydes, serving as a molecular engineering strategy for generating a diverse array of aryl fluorenone derivatives, encompassing 4-aryl, 1,4-diaryl, 2,4-diaryl, 3,5-diaryl, 1,4,6-triaryl, 2,4,6-triaryl, and 1,4,5,7-tetraaryl fluorenones (Scheme 1c). Leveraging this efficient and concise synthetic pathway, we synthesized various 1,4-diaryl SBFs with distinct structural features (Scheme 1d).
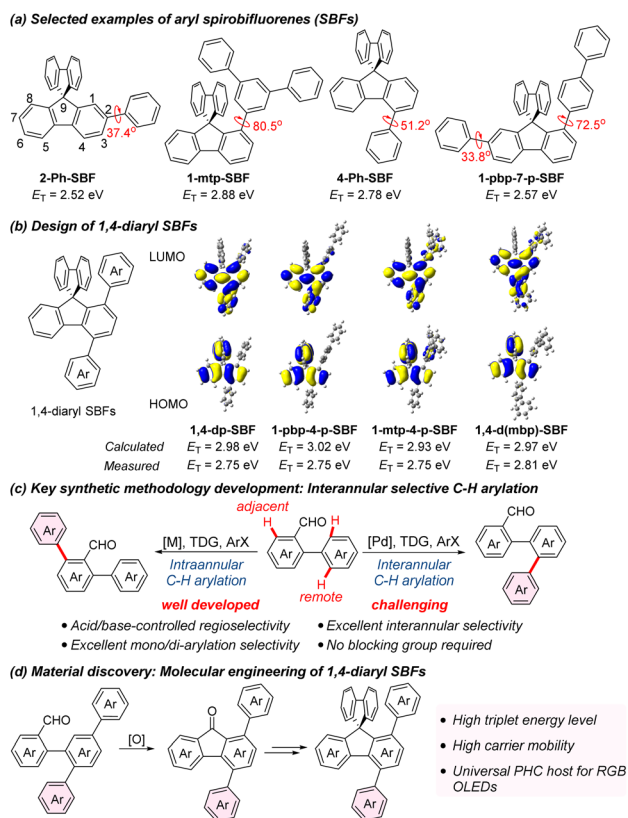

Scheme 1 Design and synthesis of 1,4-diaryl spirobifluorenes (1,4-diaryl SBFs) *via* interannular selective C–H arylation. For the structures of 1,4-diaryl SBFs see Scheme 4. TDG = transient directing group.

Subsequently, we investigated their electronic and physical properties as well as performance as host materials in PhOLEDs.
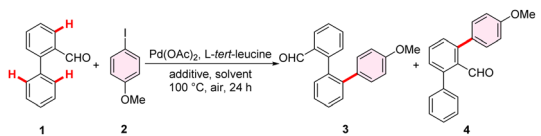
Results and discussion

Synthetic methodology development

Transition metal-catalyzed C–H arylation has emerged as a pivotal strategy for accomplishing aryl–aryl coupling and constructing fluorene structures.[18–25] Recently, our research group successfully developed an Ir(iii)-catalyzed intraannular *ortho*-C–H diarylation/annulation of benzoic acids, leading to the construction of SBFs with C1-aryl substitution.[6] However, it is not suitable to construct 4-aryl SBFs or 1,4-diaryl SBFs *via* this Ir(iii)-catalyst system owing to product substitution patterns and/or generation of inseparable regioisomeric products. In principle, the interannular *ortho*-C–H arylation of biphenyl-2-carboxylic acids or biphenyl-2-formaldehydes can offer a convenient route to synthesize 4-aryl SBFs. In recent years, tremendous efforts have been devoted to the remote functionalization of biaryl substrates through an interannular directed C–H activation strategy.[26–31] Nevertheless, the selective interannular over intraannular *ortho*-C–H arylation of biphenyl-2-formaldehydes as well as biphenyl-2-carboxylic acids remains a challenging task (Scheme 1c). The current compromise solution to this issue relied on (i) incorporating blocking groups at both competitive reaction sites and (ii) utilizing an alkene insertion/β-oxygen elimination/protonolysis/dehydration cascade process with strained 7-oxabenzonorbornadienes as the arylation reagents.[32,33] However, the former cannot access 4-aryl SBFs because blocking groups of biphenyl-2-formaldehyde substrates are difficult to remove. The latter only affords benzaldehydes containing binaphthyl units as the main product, which are unable to be transformed into the SBF structure.

To tackle the aforementioned synthetic problem, the interannular *ortho*-C–H arylation of biphenyl-2-carboxylic acid was initially explored. However, despite attempts with various catalyst systems, only the intraannular *ortho*-C–H arylated product was observed. Next, the interannular C–H arylation of biphenyl-2-formaldehyde (**1**) was studied instead, employing 1-iodo-4-methoxybenzene (**2**) as the arylation reagent, L-*tert*-leucine as the TDG, Pd(OAc)$_2$ as the catalyst and Ag$_2$CO$_3$ as the additive (Tables 1 and S1†). Irrespective of the use of HFIP/HOAc or TFE/HOAc, the primary product identified was the intraannular *ortho*-C–H arylated product **4** (Table 1, entries 1 and 2). Notably, the TFE/TFA system also predominantly exhibited intraannular *ortho*-C–H arylated reactivity (Table 1, entry 3). From these observations, we concluded that the addition of acid to the reaction system did not effectively promote the formation of the interannular arylated product. When HFIP or TFE was used as solvent alone, the desired product **3** could be obtained but in low yield (Table 1, entries 4 and 5). Surprisingly, the introduction of alkaline additives into the reaction system resulted in an increased conversion rate while maintaining excellent selectivity for interannular arylation (Table 1, entries 6 and 7). Specifically, the inclusion of ZnCO$_3$ as an additive and TFE as the solvent yielded a favorable outcome, enabling the

Table 1 Condition survey for interannular selective C–H arylation reactions[a]

Entry	Additive I	Additive II	Solvent	Yield of 3 (%)	Yield of 4 (%)
1	Ag$_2$CO$_3$	HOAc	HFIP	12	27
2	Ag$_2$CO$_3$	HOAc	TFE	0	22
3	Ag$_2$CO$_3$	TFA	TFE	Trace	43
4	Ag$_2$CO$_3$	—	HFIP	25	0
5	Ag$_2$CO$_3$	—	TFE	28	0
6	Ag$_2$CO$_3$	K$_2$CO$_3$	TFE	36	0
7	Ag$_2$CO$_3$	ZnCO$_3$	TFE	42	0
8	**AgTFA**	**ZnCO$_3$**	**TFE**	**72**	**0**

[a] Reaction conditions: **1** (0.20 mmol), **2** (0.30 mmol), Pd(OAc)$_2$ (10 mol%), L-*tert*-leucine (30 mol%), additives and solvent at 100 °C for 24 h under air. HFIP = 1,1,1,3,3,3-hexafluoro-2-propanol; TFE = 2,2,2-trifluoroethanol; TFA = trifluoroacetic acid.

isolation of the interannular arylated product **3** in a yield of 42% (Table 1, entry 7). Given the crucial role of silver salts in arylating reactions with iodobenzene substrates, we conducted a screening of various silver salts.[34] The results indicated that silver trifluoroacetate (AgTFA) exhibited the best reaction efficiency. The replacement of Ag$_2$CO$_3$ with AgTFA significantly improved the reaction yield, reaching 72% (Table 1, entry 8). No arylation reaction was detected in the absence of a TDG, indicating the necessity of a TDG (Table S1,† entry 17). Further optimization of the reaction parameters including palladium catalysts, oxidants, TDGs, and reaction temperatures could not significantly improve the reaction yield (Table S1†). Consequently, the optimal conditions comprised of Pd(OAc)$_2$ as the catalyst, L-*tert*-leucine as the TDG, AgTFA and ZnCO$_3$ as the additives, and TFE as the solvent.

Scope of substrates

Under optimal conditions, we explored the substrate scope of aryl iodides (Scheme 2). Various functional groups, including methoxy (**3**), methyl (**5**), phenyl (**6**), halogen (**7** and **8**, **29** and **30**), ester (**9**), formyl (**10**), and acetyl groups (**11**), were well-tolerated, affording the interannular *ortho*-C–H arylated products with excellent selectivity in moderate to good yields. Iodobiaryl substrates, such as iodo biphenyl and iodo terphenyl, worked well under the standard condition, offering possibilities for the follow-up preparation of PHC host materials (**6** and **32**). We also explored the generality of aryl aldehyde substrates. Biphenyl-2-formaldehyde substrates featuring both electron-donating groups, such as alkyl (**14**), and methoxy (**21**), and electron-withdrawing groups, such as ester (**15** and **22**), and nitro (**23**) and halogens (**19** and **20**), demonstrated successful engagement in the interannular arylation reaction. Selective arylation of 3′-aryl substituted biphenyl-2-formaldehydes yielded the desired products, which are crucial intermediates for the preparation of
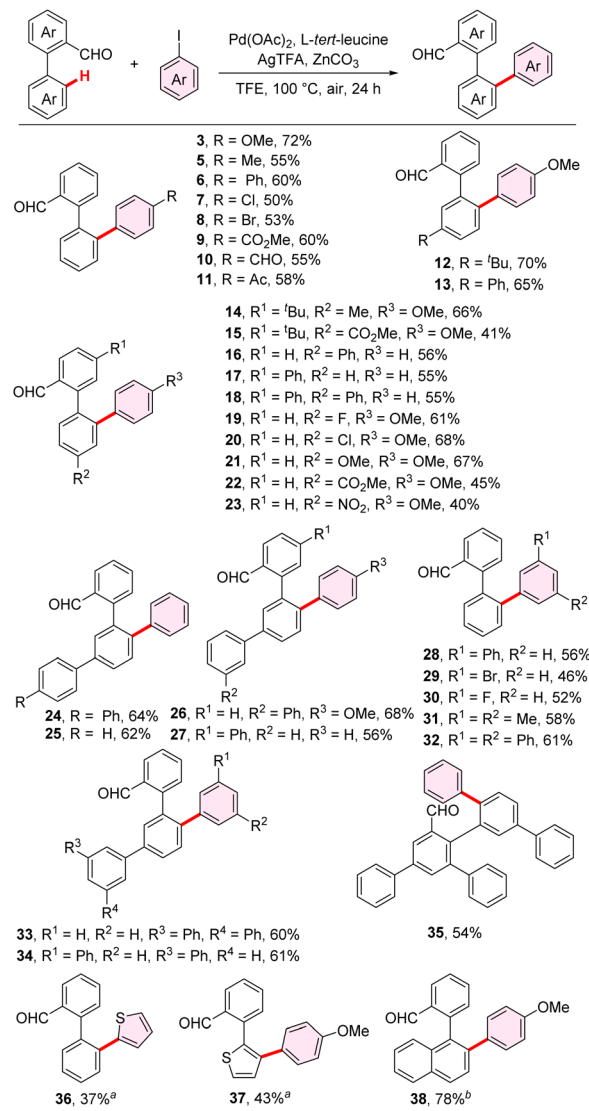
Scheme 2 Scope of substrates. Reaction conditions: bi(hetero)aryl aldehyde (0.2 mmol), aryl iodide (0.3 mmol), Pd(OAc)$_2$ (10 mol%), L-*tert*-leucine (30 mol%), AgTFA (1.5 equiv.), ZnCO$_3$ (1.0 equiv.) and TFE (1.0 mL) at 100 °C for 24 h under air. Isolated yields. [a]36 h. [b]4-Iodoanisole (0.4 mmol).

1,4-diaryl SBFs (**24, 25, 33, 34**). Their scale-up syntheses were also performed under the same conditions (Fig. S2†). Additionally, 2-(thiophen-2-yl)benzaldehyde was compatible, achieving the arylation at β-rather than α-sites of thiophene unit in a 43% isolated yield (**37**). The relatively low yield was attributed to inferior conversion rather than side reactions. Notably, 2-(naphthalen-1-yl)benzaldehyde gave the interannular arylation product in 78% yield, when increasing the amount of the iodide substrate to two equivalents (**38**).

Synthesis of multi-aryl fluorenones and 1,4-diaryl SBFs

A series of aryl fluorenones, including 4-aryl, 1,4-diaryl, 2,4-diaryl, 3,5-diaryl, 1,4,6-triaryl, 2,4,6-triaryl, and 1,4,5,7-tetraaryl fluorenones were synthesized through the intramolecular dehydrogenative arylation of aryl-substituted biphenyl-2-

formaldehyde products. This transformation was achieved in the presence of potassium persulfate and tetraethylammonium bromide (TEAB), as illustrated in Scheme 3.[35] Subsequently, 1,4-diaryl SBFs were prepared through the nucleophilic addition of *in situ* generated [1,1'-biphenyl]-2-yllithium to the carbonyl group of fluorenones, followed by intramolecular Friedel–Crafts alkylation promoted by BF$_3$ (Scheme 4).
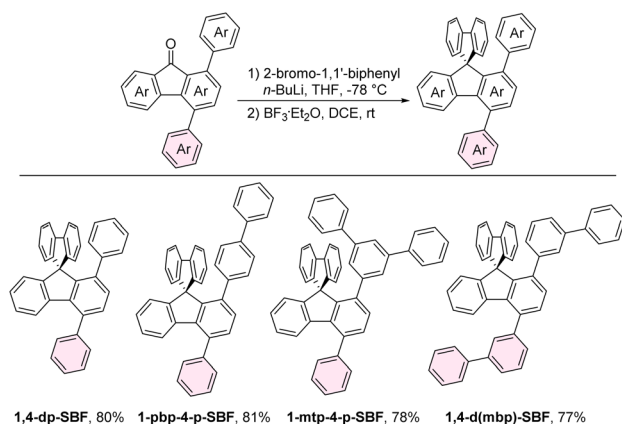
Single crystal structures

The single crystal X-ray structures and packing patterns of **1-pbp-4-p-SBF**, **1-mtp-4-p-SBF** and **1,4-d(mbp)-SBF** are depicted in Fig. 1.[36] The crystal structures reveal that the introduction of aryl group at C4 position results in a relatively large dihedral

angle between the fluorene plane and its pendant aromatic ring, with angle degrees of 47.4° for **1-pbp-4-p-SBF**, 63.5° for **1-mtp-4-p-SBF**, and 67.8° for **1,4-d(mbp)-SBF**, due to the repulsive effect between adjacent aromatic rings. Owing to the orthogonal configuration between two fluorenyl cores of SBF leading to a considerable steric hindrance at the C1 site, a large dihedral angle was observed between the C1-aromatic ring and its connected fluorene plane of SBF, estimated to be 73.6°, 78.7°, and 86.2° for **1-pbp-4-p-SBF**, **1-mtp-4-p-SBF**, and **1,4-d(mbp)-SBF**, respectively. Notably, the dihedral angles of **1-pbp-4-p-SBF** at both C1 and C4 positions are smaller than those in **1-mtp-4-p-SBF** or **1,4-d(mbp)-SBF**. Moreover, the dihedral angle of the *para*-biphenyl group at the C1 position in **1-pbp-4-p-SBF** (11.8°) is much smaller than those of *meta*-terphenyl in **1-mtp-4-p-SBF** (35.1° and 36.7°) and *meta*-biphenyl in **1,4-d(mbp)-SBF** (30.8°). The good planarity of the *para*-biphenyl structure contributes to the π···π conjugation (electronic coupling), leading to a decrease in free energy. This is a powerful driving force, which may be a reasonable explanation for the overall smaller dihedral angles of the *para*-quaterphenyl structure in **1-pbp-4-p-SBF**. By comparison, the electronic decoupling of the *meta*-connection mode may result in the overall larger dihedral angles in **1-mtp-4-p-SBF** and **1,4-d(mbp)-SBF**. In a word, the *para*-quaterphenyl structure in **1-pbp-4-p-SBF** features not only the best linearity but also the best planarity among the three molecules, possibly favorable towards organized intermolecular packing and carrier mobilities. **1-pbp-4-p-SBF**, **1-mtp-4-p-SBF**, and **1,4-d(mbp)-SBF** exhibit short distances of 3.07 Å, 3.10 Å, and 3.10 Å between the carbon atom connected to the C1 position and the non-substituted fluorene plane, respectively. The shorter distance of 3.07 Å between the intramolecular π-planes in **1-pbp-4-p-SBF**
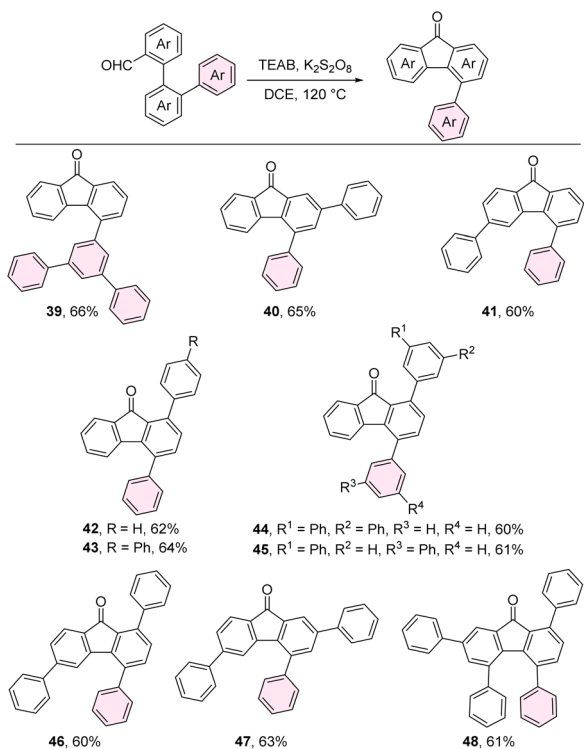
Scheme 3 Synthesis of multi-aryl fluorenones.

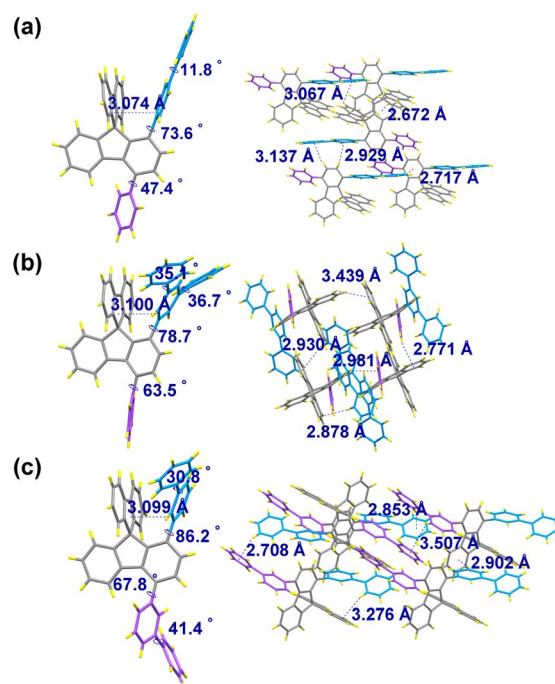Scheme 4 Synthesis of 1,4-diaryl 9,9'-spirobifluorenes.

Fig. 1 Single crystal X-ray structures and packing patterns of (a) **1-pbp-4-p-SBF**, (b) **1-mtp-4-p-SBF**, and (c) **1,4-d(mbp)-SBF**.

is beneficial to the through-space charge transfer,[37,38] which might further improve the carrier mobility. All three crystals adopt an edge-to-face packing mode stabilized by intermolecular multiple C–H···π interaction networks.

Electronic and physical properties

As depicted in Fig. 2a and summarized in Table 2, all 1,4-diaryl spirobifluorenes exhibit similar UV/vis absorption spectra. The absorption bands at 298 and 310–311 nm are closely consistent with the characteristic band of non-substituted SBF, indicating that the aryl substituents at both C1 and C4 positions have little effect on the absorption spectra. Their optical band gaps (E_g) were calculated from the onset of the absorption spectra and found to be 3.92, 3.90, 3.88, and 3.89 for **1,4-dp-SBF**, **1-pbp-4-p-SBF**, **1-mtp-4-p-SBF**, and **1,4-d(mbp)-SBF**, respectively. These

1,4-diaryl SBFs show red-shifted emission bands compared to 1-aryl substituted spirobifluorenes,[12] yet their spectra closely resemble that of the **4-Ph-SBF**.[13] These findings demonstrate that the aryl substituent attached at C1 position exerts very little influence on the emission property, attributed to the conjugation breaking at C1 position in both the ground and excited states. In contrast, C4-aryl substituents have a slight impact on the emission spectra owing to partial planarization between the C4-aromatic ring and its connected fluorene plane of SBF in the first excited state.[13] The quantum yields of these 1,4-diaryl SBFs range from 43% to 55%. The singlet energies (E_{S1}) of **1,4-dp-SBF**, **1-pbp-4-p-SBF**, **1-mtp-4-p-SBF**, and **1,4-d(mbp)-SBF** were estimated to be 3.68, 3.65, 3.65, and 3.60 eV, respectively. These four 1,4-diaryl SBFs exhibit high E_T. Calculated from the first phosphorescence peak at 77 K in toluene, the corresponding E_{T1} values are 2.75, 2.75, 2.75, and 2.81 eV for **1,4-dp-SBF**, **1-pbp-4-p-SBF**, **1-mtp-4-p-SBF**, and **1,4-d(mbp)-SBF**, respectively (Table 2 and Fig. S3a†). **1,4-dp-SBF**, **1-pbp-4-p-SBF**, and **1-mtp-4-p-SBF** containing the same phenyl substituent at their C4 positions, exhibit identical E_{T1} values. This result clearly demonstrates that the C1-aryl substituent, regardless of phenyl, *para*-biphenyl, or *meta*-terphenyl group, has almost no effect on E_T owing to the conjugation breaking. The **1,4-d(mbp)-SBF** with the *meta*-biphenyl group at C4 position shows higher E_{T1} value than the other three 1,4-diaryl SBFs, perhaps because that the electronic decoupling of the *meta*-connection mode leads to a large dihedral angle, weakening the conjugation degree of molecules in the excited state. All four 1,4-diaryl SBFs in the pure film show slightly redshifted phosphorescence emission compared to those in toluene solutions, owing to stronger intermolecular interactions in the aggregated state (Fig. S3b†). Utilizing cyclic voltammogram (CV) measurements (Fig. 2c and d), the HOMO energy levels for **1,4-dp-SBF**, **1-pbp-4-p-SBF**, **1-mtp-4-p-SBF**, and **1,4-d(mbp)-SBF** were determined to be −5.77, −5.79, −5.77, and −5.78 eV, respectively. Their LUMOs were measured at −1.74, −1.75, −1.77, and −1.77 eV, respectively.
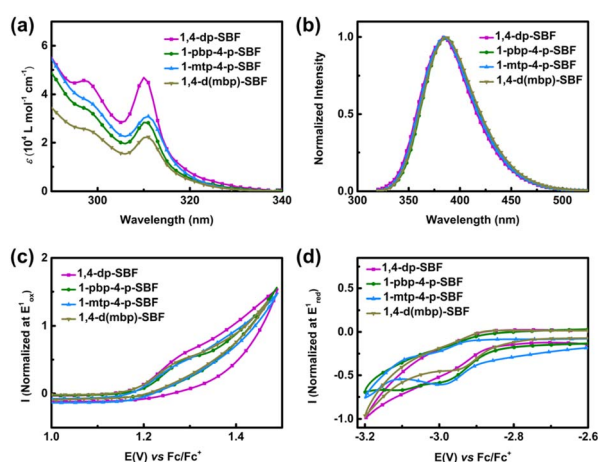

Fig. 2 (a) UV-vis absorption spectra, (b) emission spectra at 298 K in toluene, and cyclic voltammetry (CV) data: (c) in oxidation: CH₂Cl₂/[NBu₄PF₆] 0.1 M, and (d) in reduction: DMF/[NBu₄PF₆] 0.1 M; sweep rate of 100 mV⁻¹ of **1,4-dp-SBF**, **1-pbp-4-p-SBF**, **1-mtp-4-p-SBF**, and **1,4-d(mbp)-SBF**.

Table 2 Electronic and physical properties

Property	1,4-dp-SBF	1-pbp-4-p-SBF	1-mtp-4-p-SBF	1,4-d(mbp)-SBF
λ_{abs} (ε)[a] [nm]	298 (4.58)	298 (3.35)	298 (3.59)	298 (2.53)
(10⁴ L mol⁻¹ cm⁻¹)	310 (4.70)	310 (2.83)	311 (3.09)	311 (2.23)
λ_{em}[a] [nm]	384	385	386	386
E_{S1}[b] [eV]	3.68	3.65	3.65	3.60
E_{T1}[c] [eV]	2.75	2.75	2.75	2.81
E_g[d] [eV]	3.92	3.90	3.88	3.89
T_g [°C]	78	97	—	100
T_d [°C]	304	356	380	394
Φ[a] [%]	43	52	47	55
LUMO[e] [eV]	−1.74	−1.75	−1.77	−1.77
HOMO[e] [eV]	−5.77	−5.79	−5.77	−5.78
μ_h (10⁻⁵)[f] [cm² V⁻¹ S⁻¹]	1.29	3.83	1.45	1.84
μ_e (10⁻⁵)[g] [cm² V⁻¹ S⁻¹]	2.74	4.06	3.15	1.63

[a] Measured in toluene solution (1.0×10^{-5} M), where λ_{abs} is the absorption peak, λ_{em} is the photoluminescence peak at room temperature, Φ is the fluorescence quantum yield, and ε is the molar absorption coefficient in parentheses. [b] Calculated from the onset of emission at rt. [c] Calculated from the first phosphorescence peak at 77 K in toluene. [d] Calculated from the onset of the absorption spectra. [e] From CVs (CH₂Cl₂ in oxidation and DMF in reduction). [f] Hole mobility (μ_h). [g] Electron mobility (μ_e).

The thermal and morphological stabilities of host materials play a crucial role in determining the stability of OLEDs. Thermogravimetric analysis (TGA) indicates that **1,4-dp-SBF**, **1-pbp-4-p-SBF**, **1-mtp-4-p-SBF**, and **1,4-d(mbp)-SBF** possess high decomposition temperatures at 5% mass loss (T_d), ranging from 304 to 394 °C, ensuring the stability of the compounds under vacuum evaporation (Table 2 and Fig. S4†). Differential scanning calorimetry (DSC) measurements were performed for the four 1,4-diaryl SBFs between 30 and 250 °C (Table 2 and Fig. S4†). At the first heating curve, **1,4-dp-SBF**, **1-pbp-4-p-SBF**, and **1,4-d(mbp)-SBF** exhibited sharp endothermic peaks at 214 °C, 233 °C, and 221 °C, respectively, and then completely melted. These molten liquids, upon cooling to room temperature, solidified into amorphous states without undergoing recrystallization. During the second heating cycle at the same rate, the glass transition temperatures (T_g) were measured to be 78 °C, 97 °C, and 100 °C for **1,4-dp-SBF**, **1-pbp-4-p-SBF**, and **1,4-d(mbp)-SBF**, respectively. However, **1-mtp-4-p-SBF** did not exhibit melting even beyond 250 °C, and consequently, its glass transition phenomenon was not observed.

The carrier mobility and charge balance capacity of host materials have a significant impact on the performance of OLED devices.[39] Therefore, prior to assessing the electroluminescence (EL) performance of these host materials, hole-only devices (HODs) and electron-only devices (EODs) were fabricated to investigate their charge transport properties (Fig. S5† and Table 2). All four 1,4-diaryl SBFs exhibit relatively high carrier mobilities for both hole and electron, among which **1-pbp-4-p-SBF** displays the highest mobility and excellent charge balance with a hole mobility of 3.83×10^{-5} cm^2 V^{-1} s^{-1} and an electron mobility of 4.06×10^{-5} cm^2 V^{-1} s^{-1}, demonstrating that the *para*-biphenyl substituent at the C1 position contributes to carrier mobility, consistent with our earlier speculation.

To gain deeper insight into the charge transport properties of 1,4-diaryl SBFs, the transfer integrals of **1-pbp-4-p-SBF**, **1-mtp-4-p-SBF**, and **1,4-d(mbp)-SBF** were estimated by density functional theory (DFT) calculation at the B3LYP/DZ level using the Multiwfn (Fig. 3).[40] In all crystals, **1-pbp-4-p-SBF** possesses the most orderly arrangement, because of multiple strong C–H⋯π interactions between substituted and non-substituted fluorenes in adjacent molecules. The relatively weak intermolecular C–H⋯π interactions between the *para*-biphenyl at C1 position and non-substituted fluorene further strengthen the orderly arrangement. Therefore, **1-pbp-4-p-SBF** displays the largest transfer integrals with $t_1 = 44$ meV, $t_2 = 38$ meV, and $t_3 = 10$ meV for holes, as well as $t_1 = 14$ meV, $t_2 = 4$ meV, and $t_3 = 5$ meV for electrons, consistent with its high carrier mobilities. In contrast, the intermolecular arrangements of **1-mtp-4-p-SBF** and **1,4-d(mbp)-SBF** are less orderly, therefore resulting in smaller transfer integrals and lower carrier mobilities. These results suggest that the better linear and planar *para*-quaterphenyl structure of **1-pbp-4-p-SBF** significantly facilitates more orderly intermolecular packing compared to the *para*-terphenyl structures of **1-mtp-4-p-SBF** and **1,4-d(mbp)-SBF**, therefore leading to higher carrier mobilities, which further indicates that the molecular design strategy herein proposed for PHC hosts was successful.
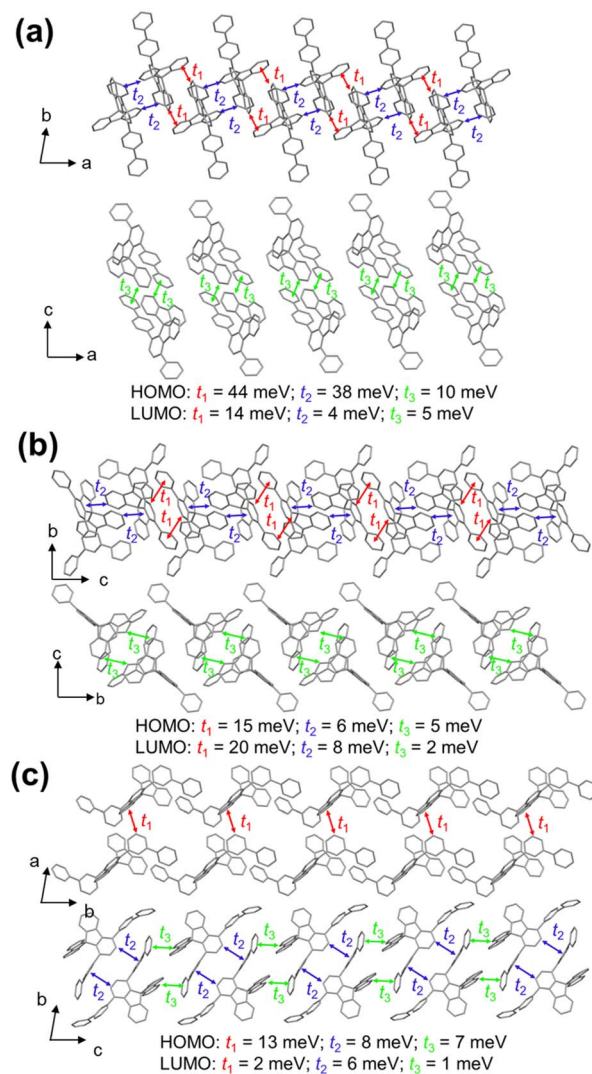

Fig. 3 HOMO and LUMO transfer integral spatial distributions in the equilibrium crystal structures of (a) **1-pbp-4-p-SBF**, (b) **1-mtp-4-p-SBF**, and (c) **1,4-d(mbp)-SBF**.

Electroluminescence performances

We assembled RGB PhOLEDs employing widely used bis[4-methyl-2-(3,5-dimethylphenyl)quinoline] tetramethyl heptadionate iridium(III) (**Ir(mphmq)₂(tmd)**) as a red phosphor, bis(2-phenylpyridine) iridium(III)-acetylacetonate (**Ir(ppy)₂(acac)**) as a green phosphor, and bis(3,5-difluoro-2-(2-pyridyl)phenyl) 2-carboxypyridyl iridium(III) (FIrpic) as a blue phosphor (Fig. 4 and Table 3). Each of the RGB devices exhibited identical EL emission spectra, affirming effective energy transfer from host to emitter. The electroluminescence of Firpic in the four hosts are slightly different, due to its dual-emission characteristic.[41] In the blue device, the best performance was achieved using **1-pbp-4-p-SBF** as the host material, attaining a maximum external quantum efficiency (EQE$_{max}$) of 22.5%. **1-pbp-4-p-SBF** also showed excellent performance as the host of green PhOLEDs with EQE$_{max}$ of 26.1% and minimal efficiency roll-off. At luminance levels of 1000 cd m^{-2} and 5000 cd m^{-2}, the EQE values are well-preserved at 25.4% and 23.0%, respectively (Tables 3
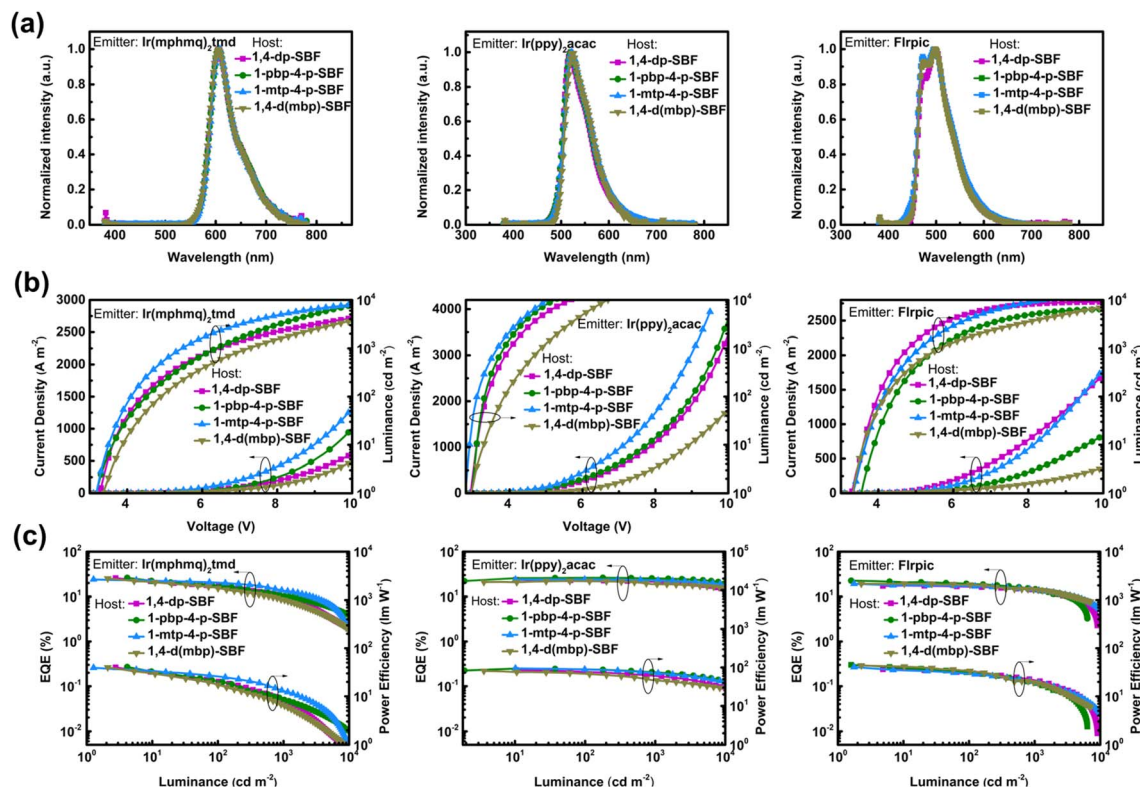
Fig. 4 OLED device performances. (a) Electroluminescence spectra of red (left), green (middle), and blue (right) PhOLEDs at the luminance of 1000 cd m^{-2}. (b) Luminance and current density *versus* voltage curves of red (left), green (middle), and blue (right) PhOLEDs devices. (c) EQE and power efficiency *versus* luminance curves of red (left), green (middle), and blue (right) PhOLEDs devices.

Table 3 Summary of OLED performances

Emitter	Host	EL$_{peak}$ [nm]	V_{on}^{a} [V]	CIE^{b} [x, y]	EQE$_{max}$/100/1000^{c} [%]	PE$_{max}$/100/1000^{d} [lm W^{-1}]
Ir(mphmq)$_2$tmd	**1,4-dp-SBF**	606	3.4	[0.63, 0.36]	25.7/16.8/10.6	40.1/20.2/8.3
	1-pbp-4-p-SBF	605	3.4	[0.63, 0.37]	26.0/17.5/10.2	40.8/20.7/8.5
	1-mtp-4-p-SBF	608	3.3	[0.64, 0.36]	24.0/20.3/13.3	39.2/26.0/12.7
	1,4-d(mbp)-SBF	606	3.5	[0.63, 0.37]	25.1/15.2/8.6	39.8/17.2/6.6
Ir(ppy)$_2$acac	**1,4-dp-SBF**	520	3.0	[0.30, 0.63]	23.6/22.8/21.4	86.4/76.3/60.8
	1-pbp-4-p-SBF	521	3.0	[0.31, 0.63]	26.1/26.0/25.4	93.8/89.7/76.0
	1-mtp-4-p-SBF	522	2.9	[0.32, 0.63]	24.0/24.0/22.8	94.8/89.2/70.9
	1,4-d(mbp)-SBF	523	3.0	[0.31, 0.64]	22.0/21.9/18.9	81.2/69.5/46.3
Flrpic	**1,4-dp-SBF**	497	3.4	[0.18, 0.42]	17.5/16.5/13.9	36.4/30.7/21.6
	1-pbp-4-p-SBF	498	3.5	[0.18, 0.41]	22.5/19.2/14.5	45.1/31.6/18.8
	1-mtp-4-p-SBF	495	3.4	[0.19, 0.39]	19.2/17.0/14.0	40.4/29.8/19.7
	1,4-d(mbp)-SBF	498	3.6	[0.18, 0.41]	19.3/18.3/14.2	43.6/33.6/19.6

^{a} Turn-on voltage. ^{b} Commission internationale de I'Eclairage (CIE). ^{c} Maximum external quantum efficiency and external quantum efficiency at the luminance of 100 cd m^{-2} and 1000 cd m^{-2}. ^{d} Maximum power efficiency and power efficiency at the luminance of 100 cd m^{-2} and 1000 cd m^{-2}.

and S5†). These favorable outcomes could be attributed to its high carrier mobilities and excellent charge balance. Furthermore, the red PhOLED using **1-pbp-4-p-SBF** as the host also demonstrated superior performance, achieving an EQE$_{max}$ of 26.0%.

Conclusions

In summary, we have developed a highly efficient palladium catalyst system for achieving the interannular selective C–H arylation of bi(hetero)aryl-2-formaldehydes, facilitating the synthesis of various aryl fluorenone derivatives, including 4-aryl, 1,4-diaryl, 2,4-diaryl, 3,5-diaryl, 1,4,6-triaryl, 2,4,6-triaryl, and 1,4,5,7-tetraaryl fluorenones. Leveraging this streamlined pathway, we have prepared four 1,4-diaryl SBF derivatives and investigated their potential as universal PHC hosts for RGB PhOLEDs. The design concept of introducing a linear structure into the orthogonal configuration of SBF is proposed. The four 1,4-diaryl SBFs as the pivotal model molecules successfully verify this concept. The coordination of molecular linearity and

orthogonality endows **1-pbp-4-p-SBF** with excellent performances as a universal PHC host. This work not only underscores the great potential of 1,4-diaryl SBFs as PHC hosts but also presents an expedited route to access these hosts.

Data availability

All data supporting the findings of this study are available within the article and its ESI file.†

Author contributions

Q. Li carried out most parts of the experiments. Z. Yu analyzed the partial data. Q. Liu and Y. Guo performed some of the synthesis. Z. Fu performed DFT calculations. J. Lan designed and directed the project. J. Lan, Z. Bin, Y. Yang, Z. Yu and Q. Li wrote the manuscript. All authors contributed to discussions.

Conflicts of interest

There are no conflicts to declare.

Acknowledgements

Notes and references

1 T. P. I. Saragi, T. Spehr, A. Siebert, T. Fuhrmann-Lieker and J. Salbeck, *Chem. Rev.*, 2007, **107**, 1011–1065.
2 R. Pudzich, T. Fuhrmann-Lieker and J. Salbeck, *Adv. Polym. Sci.*, 2006, **199**, 83–142.
3 Y. Tao, C. Yang and J. Qin, *Chem. Soc. Rev.*, 2011, **40**, 2943–2970.
4 C. Poriel and J. Rault-Berthelot, *J. Mater. Chem. C*, 2017, **5**, 3869–3897.
5 Y. Jiang, Y.-Y. Liu, X. Liu, H. Lin, K. Gao, W.-Y. Lai and W. Huang, *Chem. Soc. Rev.*, 2020, **49**, 5885–5944.
6 Y. Luo, Z. Liu, G. Yang, T. Wang, Z. Bin, J. Lan, D. Wu and J. You, *Angew. Chem., Int. Ed.*, 2021, **60**, 18852–18859.
7 Q. Wang, F. Lucas, C. Quinton, Y.-K. Qu, J. Rault-Berthelot, O. Jeannin, S.-Y. Yang, F.-C. Kong, S. Kumar, L.-S. Liao, C. Poriel and Z.-Q. Jiang, *Chem. Sci.*, 2020, **11**, 4887–4894.
8 C. Poriel, L. Sicard and J. Rault-Berthelot, *Chem. Commun.*, 2019, **55**, 14238–14254.
9 C. Poriel and J. Rault-Berthelot, *Acc. Mater. Res.*, 2022, **3**, 379–390.
10 S. Thiery, C. Declairieux, D. Tondelier, G. Seo, B. Geffroy, O. Jeannin, R. Métivier, J. Rault-Berthelot and C. Poriel, *Tetrahedron*, 2014, **70**, 6337–6351.
11 L. Sicard, C. Quinton, J.-D. Peltier, D. Tondelier, B. Geffroy, U. Biapo, R. Métivier, O. Jeannin, J. Rault-Berthelot and C. Poriel, *Chem.–Eur. J.*, 2017, **23**, 7719–7727.
12 F.-C. Kong, Y.-L. Zhang, C. Quinton, N. McIntosh, S.-Y. Yang, J. Rault-Berthelot, F. Lucas, C. Brouillac, O. Jeannin, J. Cornil, Z.-Q. Jiang, L.-S. Liao and C. Poriel, *Angew. Chem., Int. Ed.*, 2022, **61**, e202207204.
13 S. Thiery, D. Tondelier, C. Declairieux, G. Seo, B. Geffroy, O. Jeannin, J. Rault-Berthelot, R. Métivier and C. Poriel, *J. Mater. Chem. C*, 2014, **2**, 4156–4166.
14 L.-S. Cui, Y.-M. Xie, Y.-K. Wang, C. Zhong, Y.-L. Deng, X.-Y. Liu, Z.-Q. Jiang and L.-S. Liao, *Adv. Mater.*, 2015, **27**, 4213–4217.
15 X. Tang, Y. Li, Y.-K. Qu, C.-C. Peng, A. Khan, Z.-Q. Jiang and L.-S. Liao, *Adv. Funct. Mater.*, 2020, **30**, 1910633.
16 Y. Wang, J. H. Yun, L. Wang and J. Y. Lee, *Adv. Funct. Mater.*, 2021, **31**, 2008332.
17 C. Poriel and J. Rault-Berthelot, *Adv. Funct. Mater.*, 2021, **31**, 2010547.
18 C. Liu, J. Yuan, M. Gao, S. Tang, W. Li, R. Shi and A. Lei, *Chem. Rev.*, 2015, **115**, 12138–12204.
19 Q.-Z. Zheng and N. Jiao, *Chem. Soc. Rev.*, 2016, **45**, 4590–4627.
20 Y. Yang, J. Lan and J. You, *Chem. Rev.*, 2017, **117**, 8787–8863.
21 Y. Wei, P. Hu, M. Zhang and W. Su, *Chem. Rev.*, 2017, **117**, 8864–8907.
22 Y.-F. Zhang and Z.-J. Shi, *Acc. Chem. Res.*, 2019, **52**, 161–169.
23 B. Li, A. I. M. Ali and H. Ge, *Chem*, 2020, **6**, 2591–2657.
24 T. Dalton, T. Faber and F. Glorius, *ACS Cent. Sci.*, 2021, **7**, 245–261.
25 Y. Yang, Y. Wu, Z. Bin, C. Zhang, G. Tan and J. You, *J. Am. Chem. Soc.*, 2024, **146**, 1224–1243.
26 G. Liao, T. Zhang, Z.-K. Lin and B.-F. Shi, *Angew. Chem., Int. Ed.*, 2020, **59**, 19773–19786.
27 C.-X. Liu, W.-W. Zhang, S.-Y. Yin, Q. Gu and S.-L. You, *J. Am. Chem. Soc.*, 2021, **143**, 14025–14040.
28 G. Liao, B. Li, H.-M. Chen, Q.-J. Yao, Y.-N. Xia, J. Luo and B.-F. Shi, *Angew. Chem., Int. Ed.*, 2018, **57**, 17151–17155.
29 G. Liao, Q.-J. Yao, Z.-Z. Zhang, Y.-J. Wu, D.-Y. Huang and B.-F. Shi, *Angew. Chem., Int. Ed.*, 2018, **57**, 3661–3665.
30 U. Dhawa, C. Tian, T. Wdowik, J. C. A. Oliveira, J. Hao and L. Ackermann, *Angew. Chem., Int. Ed.*, 2020, **59**, 13451–13457.
31 H.-M. Chen, G. Liao, C.-K. Xu, Q.-J. Yao, S. Zhang and B.-F. Shi, *CCS Chem.*, 2021, **3**, 455–465.
32 J. Zhang, J. Fan, Z. Guo, Y. Wu, J. Wu and M. Xie, *Adv. Synth. Catal.*, 2022, **364**, 3589–3599.
33 G. Liao, H.-M. Chen, Y.-N. Xia, B. Li, Q.-J. Yao and B.-F. Shi, *Angew. Chem., Int. Ed.*, 2019, **58**, 11464–11468.
34 R. L. de Carvalho, E. B. T. Diogo, S. L. Homölle, S. Dana, E. N. da Silva Júnior and L. Ackermann, *Chem. Soc. Rev.*, 2023, **52**, 6359–6378.
35 Z. Shi and F. Glorius, *Chem. Sci.*, 2013, **4**, 829–833.

36 CCDC 2303140 (1,4-d(mbp)-SBF), 2303142 (**1-mtp-4-p-SBF**) and 2303143 (**1-pbp-4-p-SBF**) contain the supplementary crystallographic data for this paper. These data can be obtained free of charge from the Cambridge Crystallographic Data Centre.

37 X. Tang, L.-S. Cui, H.-C. Li, A. J. Gillett, F. Auras, Y.-K. Qu, C. Zhong, S. T. E. Jones, Z.-Q. Jiang, R. H. Friend and L.-S. Liao, *Nat. Mater.*, 2020, **19**, 1332–1338.

38 X.-Q. Wang, S.-Y. Yang, Q.-S. Tian, C. Zhong, Y.-K. Qu, Y.-J. Yu, Z.-Q. Jiang and L.-S. Liao, *Angew. Chem., Int. Ed.*, 2021, **60**, 5213–5219.

39 A. Yoshii, Y. Onaka, K. Ikemoto, T. Izumi, S. Sato, H. Kita, H. Taka and H. Isobe, *Chem.–Asian J.*, 2020, **15**, 2181–2186.

40 T. Lu and F. Chen, *J. Comput. Chem.*, 2012, **33**, 580–592.

41 E. Baranoff and B. F. E. Curchod, *Dalton Trans.*, 2015, **44**, 8318–8329.